7742–7754 *Nucleic Acids Research, 2016, Vol. 44, No. 16* *Published online 13 June 2016*
doi: 10.1093/nar/gkw515

Triplex structures induce DNA double strand breaks via replication fork collapse in NER deficient cells

Meetu Kaushik Tiwari[1], Nneoma Adaku[1], Natoya Peart[1] and Faye A. Rogers[1,2,*]

[1]Department of Therapeutic Radiology, Yale School of Medicine, New Haven, CT 06520, USA and [2]Yale Cancer Center, Yale School of Medicine, New Haven, CT 06520, USA

Received December 30, 2015; Revised May 27, 2016; Accepted May 31, 2016

ABSTRACT

Structural alterations in DNA can serve as natural impediments to replication fork stability and progression, resulting in DNA damage and genomic instability. Naturally occurring polypurine mirror repeat sequences in the human genome can create endogenous triplex structures evoking a robust DNA damage response. Failures to recognize or adequately process these genomic lesions can result in loss of genomic integrity. Nucleotide excision repair (NER) proteins have been found to play a prominent role in the recognition and repair of triplex structures. We demonstrate using triplex-forming oligonucleotides that chromosomal triplexes perturb DNA replication fork progression, eventually resulting in fork collapse and the induction of double strand breaks (DSBs). We find that cells deficient in the NER damage recognition proteins, XPA and XPC, accumulate more DSBs in response to chromosomal triplex formation than NER-proficient cells. Furthermore, we demonstrate that XPC-deficient cells are particularly prone to replication-associated DSBs in the presence of triplexes. In the absence of XPA or XPC, deleterious consequences of triplex-induced genomic instability may be averted by activating apoptosis via dual phosphorylation of the H2AX protein. Our results reveal that damage recognition by XPC and XPA is critical to maintaining replication fork integrity and preventing replication fork collapse in the presence of triplex structures.

INTRODUCTION

The generation of aberrant DNA replication forks is a major source of the mutations and chromosomal rearrangements that are associated with pathological disease. Since replicating DNA is prone to error, replication stress in the form of slowing or stalling of fork progression has serious implications for genome stability. Replication stress can occur in regions of the genome that are intrinsically difficult to replicate due to DNA sequence patterns, including trinucleotide, inverted, mirror and direct tandem repeats, which can often adapt secondary DNA structures (1). The process of replication denatures the DNA duplex and exposes long single-stranded regions at the fork, particularly during lagging strand synthesis, which provides an environment conducive to the formation of non-B structures. Conditions that alter replication fork structure during DNA synthesis can prime the region for chromosomal breakage, thus becoming a major source of spontaneous genomic instability, and consequently driving malignant transformation of precancerous cells. Therefore, replication checkpoints monitor fork progression and trigger cellular responses aimed at preserving genomic integrity. Cells can either activate DNA repair pathways to repair the damage in replicating DNA or initiate programmed cell death (2,3).

Non-canonical secondary DNA structures such as cruciforms, hairpins, H-DNA (triplex) and Z-DNA are formed at specific repetitive DNA sequences and can affect the progression of DNA replication forks (2,4,5). Under many circumstances, replication-associated helicases can resolve non-B conformations created in front of the progressing polymerase (6,7). However, if the altered helical structure is unresolved, it can initiate a stalled replication fork, leading to fork collapse and DNA double strand breaks (DSBs). The continuation of DNA synthesis past non-B DNA structures has been proposed as a key contributor to the generation of the expanded repeats responsible for the development of human diseases and hereditary disorders (2,4). For example, Friedreich's ataxia is an autosomal recessive neurodegenerative disorder caused by repeat expansion. Studies from several labs have revealed that the GAA repeat element in the first intron of the frataxin gene is capable of forming an intramolecular triplex (8). The molecular mechanism of repeat expansion has been attributed to triplex formation, which stalls replication fork progression and adds extra repeats during replication fork restart (9,10). Replication inhibition caused by triplet repeats and triple helices has also been reported through the use of plasmids containing genes associated with other hereditary disorders caused by the expansion of microsatellite DNA repeats (11–13).

*To whom correspondence should be addressed. Tel: +1 203 737 3658; Fax: +1 203 785 7482; Email: faye.rogers@yale.edu

However, none of these studies focused on replication stress and its effect on genomic integrity in the presence of multiple chromosomal triplex structures.

Cells have evolved several mechanisms to process the recurrent challenge of altered helical structures. The nucleotide excision repair (NER) pathway is responsible for the removal of bulky, helix-distorting lesions, including altered helical structures created by triplex formation (14–16). The NER protein XPC, complexed with hHR23B, serves as a DNA damage sensor and repair recruitment factor. The major function of XPC is to recognize helix-distorting lesions located in a transcriptionally inactive genome or the non-transcribed strand of actively transcribed genes. Another NER protein, XPA, verifies the damage in an open DNA conformation and coordinates the assembly of the remaining repair machinery. Human replication protein A (RPA) and XPA have been reported to form a DNA recognition complex with greater specificity for damaged DNA than XPA alone (17,18). Replication stress usually results in the formation of stretches of single-stranded DNA (ssDNA) as the replicative helicase continues to unwind the parental DNA after the polymerase has stalled. RPA binds to the excessive ssDNA that is generated as a result of replication stress and generates the signal that activates the replication stress response (19). Notably, RPA has a compromised binding affinity for DNA that is composed of repetitive purine sequences (20). Both XPC-hHR23B and XPA-RPA complexes have been shown to recognize triplex structures and triplex-directed psoralen crosslinks *in vitro* using DNA substrates (17,21). Since triplex DNA is recognized and repaired by the NER pathway, it is important to investigate the role of NER in resolving replication stress induced by altered helical structures.

Synthetic triplex DNA can be generated when triplex-forming oligonucleotides (TFOs) bind as third strands in the major groove of duplex DNA at polypurine/polypyrimidine regions via Hoogsteen hydrogen bonds. TFOs represent an excellent model to study the biological effects of chromosomal triplex formation, as these molecules have been shown to activate recombination and DNA repair in addition to inducing genomic instability (22–24). We have previously reported that TFOs can induce DNA DSBs and activate apoptosis in cells containing multiple chromosomal triplex target sites (25). To better understand the mechanism responsible for the generation of TFO-induced DSBs, we investigated the role of NER damage recognition proteins in processing triplex-induced DNA damage. In the current study, we determined that TFOs induce replication stress by stalling replication fork progression. XPC- and XPA-deficient cells had increased sensitivity to triplex-mediated replication fork collapse, with eventual induction of DNA DSBs. In the absence of triplex-initiated DNA damage recognition by XPC or XPA, cells activated apoptosis through dual phosphorylation of H2AX at residues serine 139 (S139) and tyrosine 142 (Y142), thus averting genomic instability. Our present study reveals the important roles of XPC and XPA in the response to triplex-induced DNA replication stress. This study also provides evidence that triplex formation can induce NER-independent DSBs by stalling DNA replication forks.

MATERIALS AND METHODS

Oligonucleotides

Oligonucleotides were synthesized by Midland Certified Reagent Co., Inc. and were purified by reversed-phase HPLC. To resist 3′-exonuclease activity, oligonucleotides were designed with a 3′-amino-modifier C7 CPG (Glen Research). The 30-mer TFO, AG30 was synthesized with the sequence 5′-AGGAAGGGGGGGGTGGTGGGGGAGGGGGAG-3′ and has been previously shown to bind with high affinity to a polypurine/polypyrimidine site located at positions 167–196 in the *supFG1* reporter gene (24). The control mixed-sequence oligonucleotide MIX30 has the following sequence: 5′-AGTCAGTCAGTCAGTCAGTCAGTCAGTCAG-3′.

Cell lines and transfection

Mouse embryonic fibroblast (MEF) cell lines were derived from transgenic mice carrying the *supFG1* reporter vector as a transgene in addition to targeted disruptions in the NER genes XPA ($XPA^{-/-}$) or XPC ($XPC^{-/-}$). A similar cell line containing the *supFG1* gene was derived from wild-type (WT) mice and used for comparison. Cells were grown in DMEM medium (Invitrogen) supplemented with 10% fetal bovine serum (FBS) (Invitrogen) and were maintained at 37°C in a humidified incubator with 5% CO_2. On the day before transfection, cells were seeded in six-well plates at a density of 2–3 $\times$ 10^5 cells per well. Cells were transfected with 2 μg of AG30 or MIX30 using the transfection reagent Oligofectamine (Invitrogen) as per manufacturer's instructions.

Western blotting

Floating and adherent cells were collected. Cell pellets were lysed with RIPA buffer, and 30–50 μg of total protein per sample was resolved by SDS-PAGE. Proteins were detected by a standard immunoblot protocol using the following primary antibodies: cleaved PARP, γH2AX (Cell Signaling Technology), p-H2AX (tyrosine 142; EMD Millipore), tubulin (clone B-512; Sigma) and GAPDH-HRP (Proteintech). Each experiment was carried out three times, and representative Western blots are shown.

Chromatin immunoprecipitation assay (ChIP)

Specific recruitment of XPA, XPC and RAD51 to the triplex site was evaluated using ChIP assays as previously described (26). Wild-type MEFs were transfected with AG30 or MIX30, and cells were collected 4 h and 6 h post-transfection. Chromatin immunoprecipitation (ChIP) was performed using the following antibodies: RAD51 (H-92, Santa Cruz), XPC (H-300, Santa Cruz), IgG (Jackson Immunoresearch Lab) and XPA (14). Samples were subjected to polymerase chain reaction (PCR) using the Advantage 2 PCR kit (Clontech) and amplified in an Eppendorf thermal cycler with the following settings: initial denaturation for 5 min at 95°C and 40 cycles at 95°C for 1 min, 1 min at

55°C and 1 min at 72°C. The primers utilized in these studies were: Primer J1, 5′- ACC TTC GAA GTC GAT GAC GGC AG and Primer J2, 5′- AGC GGA TAA CAA TTT CAC ACA GG. The PCR products were resolved on a 1.5% agarose gel and visualized by ethidium bromide staining using a BIORAD Chemidoc imaging system. The band intensity of the PCR products was quantified using Image Lab (BIORAD). The relative enrichment of the PCR products was determined via normalization against input followed by normalization to the untreated samples.

Apoptosis analysis

Cells (2×10^5) were seeded in six-well plates 24 h prior to treatment with either AG30 or MIX30 (2 μg). Post-treatment analysis was performed using the Annexin V-FITC/PI apoptosis detection kit (BD Pharmingen) according to the manufacturer's protocol. Apoptotic frequency was calculated as the combined percentage of early and late apoptotic cells. Data analysis was performed using FlowJo software.

Immunofluorescence

MEFs were seeded onto UV-irradiated coverslips and were treated for 24 h with either AG30, MIX30 or a mock transfection. Cells were processed 24 h post-transfection, fixed with 4% formaldehyde and then incubated with ice-cold 100% methanol followed by a methanol and acetic acid solution (1:1) for 20 min at −20°C. After washing with phosphate buffered saline (PBS), cells were blocked with blocking buffer (4% BSA, 0.2% Triton X-100 in PBS) for 30 min and then incubated overnight with the following primary antibodies: γH2AX (1:500; Cell Signaling), 53BP1 (1:100; Santa Cruz), RAD51 (Santa Cruz) and pRPA32 (Bethyl Laboratories) in blocking buffer at 4°C. After three washes, cells were incubated with secondary antibodies Alexa 488 F(ab′)2 fragment goat anti-rabbit IgG or Alexa 568 F(ab′)2 fragment goat anti-mouse IgG (1:1000; Molecular Probes) for 1 h at room temperature. Cells were then mounted on microscope glass slides with anti-fade mounting media containing DAPI (Life Technologies), and pictures were taken with a Leica SP5 microscope. pRPA32 foci were detected using the protocol described by Mirzoeva and Petrini (27).

Comet assay

Neutral comet assays were performed 24 h post-transfection as per the manufacturer's instructions (Trevigen) with the adjustment of 3.5×10^5 cells/ml cell suspension and 30 min electrophoresis. Additionally, alkaline comet assays were performed using 300 mM NaOH alkaline unwinding and electrophoresis solution. Comets were visualized using an Axiovert 200 microscope and analyzed with CometScore software. Approximately 100–200 comets were analyzed per experiment. Results were expressed as mean tail moment.

BrdU immunofluorescence and flow cytometry

Unsynchronized cells were treated with AG30 or MIX30 (2 μg), followed by a 20 min incubation with BrdU (10 μM). Treated cells were collected and washed twice with PBS before fixation and incubation with 70% ethanol for 10 min for immunofluorescence and overnight at −20°C for flow cytometry. For staining, cells were treated with 2.5 M HCl for 30 min and then neutralized for 2 min with 0.1 M sodium borate, pH 8.5. Cells were washed with PBS and blocked with 4% BSA in PBS for 30 min. For co-detection of γH2AX foci with BrdU, γH2AX antibody was added overnight at 4°C (1:500; Cell Signaling). After three washes, secondary antibody for γH2AX (Alexa 488; Molecular Probes) and anti-BrdU antibody (BD Biosciences) was added for 1 h at room temperature followed by PBS washes. Cells were mounted on microscope slides with anti-fade mounting media containing DAPI. For flow cytometry of BrdU with PI, cells were incubated with PI staining solution for 15 min. Labeled cells were analyzed using a FACSCalibur flow cytometer. Data analysis was performed using FlowJo software.

Mutagenesis assay

MEF cell lines deficient in either XPA or XPC were established with multiple copies of the *supFG1* reporter gene stably integrated into the genome. Cells were treated with either the control oligonucleotide MIX30, the TFO AG30 or a mock transfection, and genomic DNA was isolated from adherent cells 48 h post-transfection. Genomic DNA was incubated with *in vitro* packaging extracts as described previously for shuttle vector rescue and reporter gene analysis (28). Mutation frequency was calculated by dividing colorless mutant plaques by the total number of plaques counted. Standard error mean was calculated from three independent experiments.

DNA fiber analysis

DNA fiber assays were performed as previously described (29,30). WT, $XPA^{-/-}$ and $XPC^{-/-}$ cells were first labeled with 25 μM IdU for 20 min, treated with AG30 or MIX30 for 24 h, and then labeled with 250 μM CldU for 60 min. Cells were washed with PBS before resuspension at a concentration of 7.5×10^5 cells/ml in PBS. Cells (2 μl) were spotted on a glass slide and lysed with 7 μl of lysis buffer (50 mM EDTA, 0.5% SDS, 200 mM Tris-HCl, pH 7.5) for 2 min. Slides were tilted at a 15° angle to allow for the spreading of DNA fibers. For immunofluorescence, slides were immersed in methanol:acetic acid (3:1) for 10 min and then treated with 2.5 M HCl for 80 min. After PBS washes, slides were incubated with 5% BSA for 30 min at room temperature followed by overnight incubation at 4°C with primary antibodies (1:25 mouse anti-BrdU for IdU and 1:400 rat anti-BrdU for CIdU). Slides were washed with PBS and incubated with secondary antibodies (1:500 sheep anti-mouse Cy3 for IdU and 1:400 goat anti-rat Alexa Fluor 488 for CIdU) for 1 h at room temperature. Slides were washed three times and covered with coverslips with VECTASHIELD mounting media. Images were acquired at 63x magnification with a Zeiss microscope. ImageJ software was used to measure the lengths of IdU-labeled (red Cy3) or CIdU-labeled (green Alexa 488) fibers, and values were converted into micrometers. XPA and XPC proteins

were produced in the complementation studies using the pcDNA4-Flag-XPA (Addgene) and pcDNA-HA-XPC (obtained from P. Glazer) expression vectors.

Statistical analysis

Statistical analysis was performed by one-way or two-way ANOVA with the Tukey's test as post hoc. All analysis was completed using GraphPad Prism software. $****P < 0.0001$, $***P < 0.001$, $**P < 0.01$, $*P < 0.05$.

RESULTS

NER damage recognition proteins bind TFO-induced structures

Our prior studies have demonstrated that the formation of multiple triplex structures creates a severe enough alteration in the DNA double helix to generate DNA damage in the form of DSBs (25). Triplex formation has been previously shown to be recognized as DNA damage by the NER pathway. In order to elucidate the mechanism by which triplex structures induce DSBs, we used NER-deficient MEF cell lines ($XPC^{-/-}$ and $XPA^{-/-}$) to investigate the potential role of DNA damage recognition (Figure 1A). These NER-deficient cells were also engineered to contain multiple chromosomal triplex target sites. Thus, triplex structures can be synthetically generated using the TFO, AG30, which binds specifically to its polypurine target sequence (Figure 1B).

To validate that the damage recognition proteins XPA and XPC interact with the synthetic chromosomal triplex structures generated by AG30, we performed ChIP assays in the WT MEFs. PCR amplification following chromatin immunoprecipitation with either XPA or XPC antibodies using proximal primers to the target sequence revealed an enrichment of both proteins at the triplex site compared to untreated cells (Figure 1). XPA immunoprecipitated DNA fragments isolated from WT cells 6 h post TFO-treatment clearly demonstrated an enrichment of XPA (∼5-fold) at the triplex binding site relative to untreated control cells (Figure 1C and D), suggesting DNA damage-specific recruitment of XPA. However, XPC enrichment was detected at the triplex site as early as 4 h post AG30-treatment (Figure 1E and F). XPC had a greater than 9-fold enrichment at the TFO binding site compared to untreated cells. These results indicate that XPA and XPC are specifically recruited to the triplex structure and suggest that XPC is the first recognition protein at the triplex-induced damage site. Taken together, these findings confirm that TFO-induced structures are recognized as DNA damage by NER damage recognition proteins.

Triplex DNA induces replication associated DNA strand breaks

To assess whether triplex-induced DNA DSBs were associated with DNA replication, we co-immunostained NER-proficient and -deficient cells with BrdU and γH2AX, whose colocalization can be used as a marker of replication stress (31). The majority of triplex-induced γH2AX foci was present in BrdU-positive cells and thus attributed to replication-mediated DNA damage. Treatment with AG30 led to an increase in γH2AX foci formation in BrdU-positive NER-proficient and -deficient cell lines compared to treatment with the control oligonucleotide, MIX30, which is unable to form a triplex structure (Figure 2A). Mock treatment with the transfection reagent alone had minimal effect on γH2AX foci formation in BrdU-positive cells. The percentage of dual BrdU- and γH2AX-positive cells following 24 h AG30 treatment was significantly higher in the NER-deficient cell lines compared to NER-proficient cells (Figure 2B). Furthermore, replicating XPC-deficient cells (68%) accumulated more triplex-induced DNA damage than replicating XPA-deficient cells (54%) (Figure 2B).

To determine if triplex-induced replication stress correlated with the accumulation of DNA strand breaks, we performed the alkaline comet assay, which measures DNA damage resulting from both single-strand breaks (SSBs) and DSBs. We observed 24 h after AG30 treatment that the accumulation of DNA strand breaks as determined by tail moment was significantly higher in the NER-deficient cells, $XPC^{-/-}$ and $XPA^{-/-}$ compared to NER-proficient cells (Figure 2C and D). In order to determine whether the excessive DNA damage induced by triplex formation in unsynchronized replicating cells would affect cell cycle progression, we also analyzed BrdU incorporation through flow cytometry. FACS analysis revealed that the level of BrdU-positive cells (S-phase) was significantly reduced 24 h after AG30 treatment (Figure 2E). However, this reduction in the S-phase population following TFO treatment was more prevalent in $XPC^{-/-}$ cells compared to $XPA^{-/-}$ and WT (Figure 2E and Supplementary Figure S1). Triplex formation in NER-proficient cells also resulted in increased cell populations in the G1 and G2/M phases of the cell cycle. Concurrently, G1 arrest was observed in XPA-deficient AG30-treated cells in contrast to XPC-deficient cells, where G2 arrest was observed with AG30 treatment (Figure 2E).

NER deficiency attenuates nascent DNA strand length following triplex-induced DNA damage

To understand the impact of triplex formation on DNA replication in NER-deficient cells, we performed DNA fiber analysis to study replication perturbation at a single-molecule level. The DNA fiber or combing assay involves the direct measurement of DNA synthesis and has been reported to be a clear readout of replication stress (32). The general schematic for these experiments is illustrated in Figure 3A. Cells were pulse-labeled with IdU (red) followed by treatment with either MIX30 or AG30 and labeling with CldU (green). Ongoing replication can be detected by simultaneous staining of red and green DNA strands, whereas singly labeled red or green tracts indicate stalled forks and newly initiated forks, respectively. TFO-treated WT, $XPA^{-/-}$ and $XPC^{-/-}$ cells produced more stalled replication forks compared to untreated and MIX30-treated cells (Figure 3B). However, we observed that $XPC^{-/-}$ cells (64%) had a higher percentage of stalled forks compared to $XPA^{-/-}$ (52%) and WT (33%) cells (Figure 3C). This corresponds to the greater decrease in the S-phase population of XPC-deficient, TFO-treated cells as observed in the cell cycle studies (Figure 2E). We then tested the ability of XPA protein to restore the TFO-induced dam-

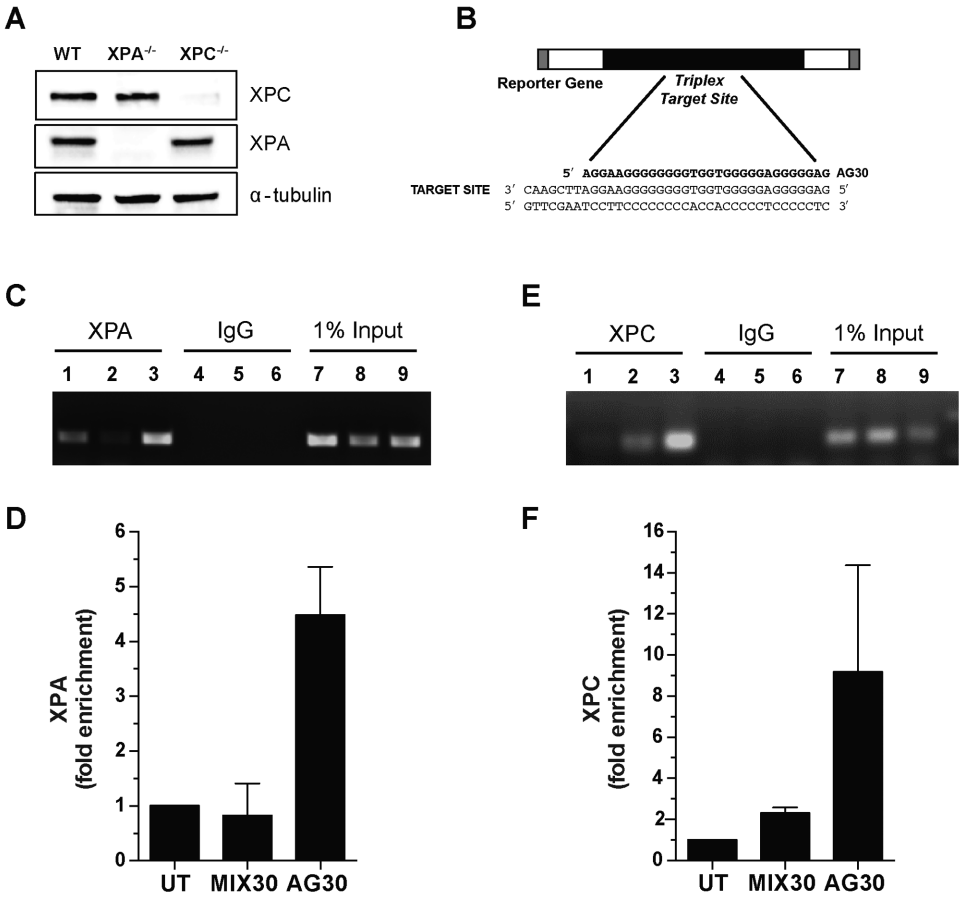

Figure 1. Association of NER damage recognition proteins with triplex DNA. (**A**) NER deficient cell lines XPA$^{-/-}$ and XPC$^{-/-}$ were analyzed for XPA and XPC protein levels and compared with WT. (**B**) Schematic for the generation of synthetic triplex structures. Triplex structures were generated using the TFO, AG30, which binds specifically to a polypurine target sequence in the *supFG1* reporter gene. (**C**) PCR analysis of ChIP assays from WT cells demonstrated an enrichment of XPA at the AG30 binding site 6 h post-treatment. Lane 1, untreated cells; Lane 2, MIX30; Lane 3, AG30. Lanes 4,5 and 6 are IgG controls for Lanes 1, 2 and 3, respectively. Lanes 7–9 represent 1% input for Lanes 1–3, respectively. (**D**) Quantification of PCR amplification from C indicated 5-fold enrichment of XPA after TFO treatment compared to untreated cells. (**E**) ChIP experiments with WT cells treated with TFO for 4 h (Lanes 1, 4, 7: untreated cells; Lanes 2, 5, 8: MIX30; Lanes 3, 6, 9: AG30) and chromatin immunoprecipatated with indicated antibodies. (**F**) Quantification of PCR products from E demonstrates greater than 9-fold enrichment of XPC after AG30 treatment compared to untreated cells.

age recognition in XPA$^{-/-}$ cells. The results show that the expression of XPA provides functional complementation in the XPA$^{-/-}$ cells (Supplementary Figure S2A and S2B). We observed a lower percentage of AG30-induced stalled forks in the XPA complemented cells (20%) compared to XPA$^{-/-}$ cells transfected with empty vector control (40%) (Figure 3D). Likewise, XPC protein was capable of complementation in the XPC-deficient cells (Supplementary Figure S2C and S2D). Expression of XPC in the XPC-deficient cells resulted in a lower percentage of triplex-induced stalled replication forks (15%), even lower than the percentage of stalled forks observed in TFO-treated WT cells (Figure 3E). These findings support the hypothesis that DNA damage recognition is important in maintaining replication fork progression in the presence of triplex structures.

Since AG30 treatment led to stalled and collapsed replication forks, we further investigated the effect of triplex structures on the maintenance of nascent DNA strands. We analyzed individual nascent DNA strands using the DNA fiber assay. Interestingly, we found that untreated NER-deficient cells (Mean ± SEM: XPA$^{-/-}$, 7 ± 0.4 μm and XPC$^{-/-}$ 6 ± 0.3 μm) spontaneously exhibited shorter mean fiber lengths of nascent DNA strands compared to untreated WT cells (9 ± 0.4 μm) (Figure 3F). TFO treatment resulted in decreased DNA fiber lengths in all cell lines. However, they were significantly shorter in the NER-deficient cells compared to WT. These results suggest that NER DNA damage recognition is critical for the maintenance of nascent DNA strands in response to triplex formation. To determine how NER deficiency affects the normal distribution of nascent DNA stability, we analyzed the DNA fiber assay based on the percentage of replication track length frequency. Not only was the DNA fiber length shorter in AG30-treated cells, but the frequency of shorter DNA fibers in the range of 1–5 μm was higher than in cells treated with the control oligonucleotide MIX30 (Figure 3G). We found that 40% and 36% of replication track lengths were in the range of 1–5 μm in untreated XPA$^{-/-}$ and XPC$^{-/-}$ cells, respectively, versus 27% in WT cells. However, TFO treatment increased the percentage of repli-

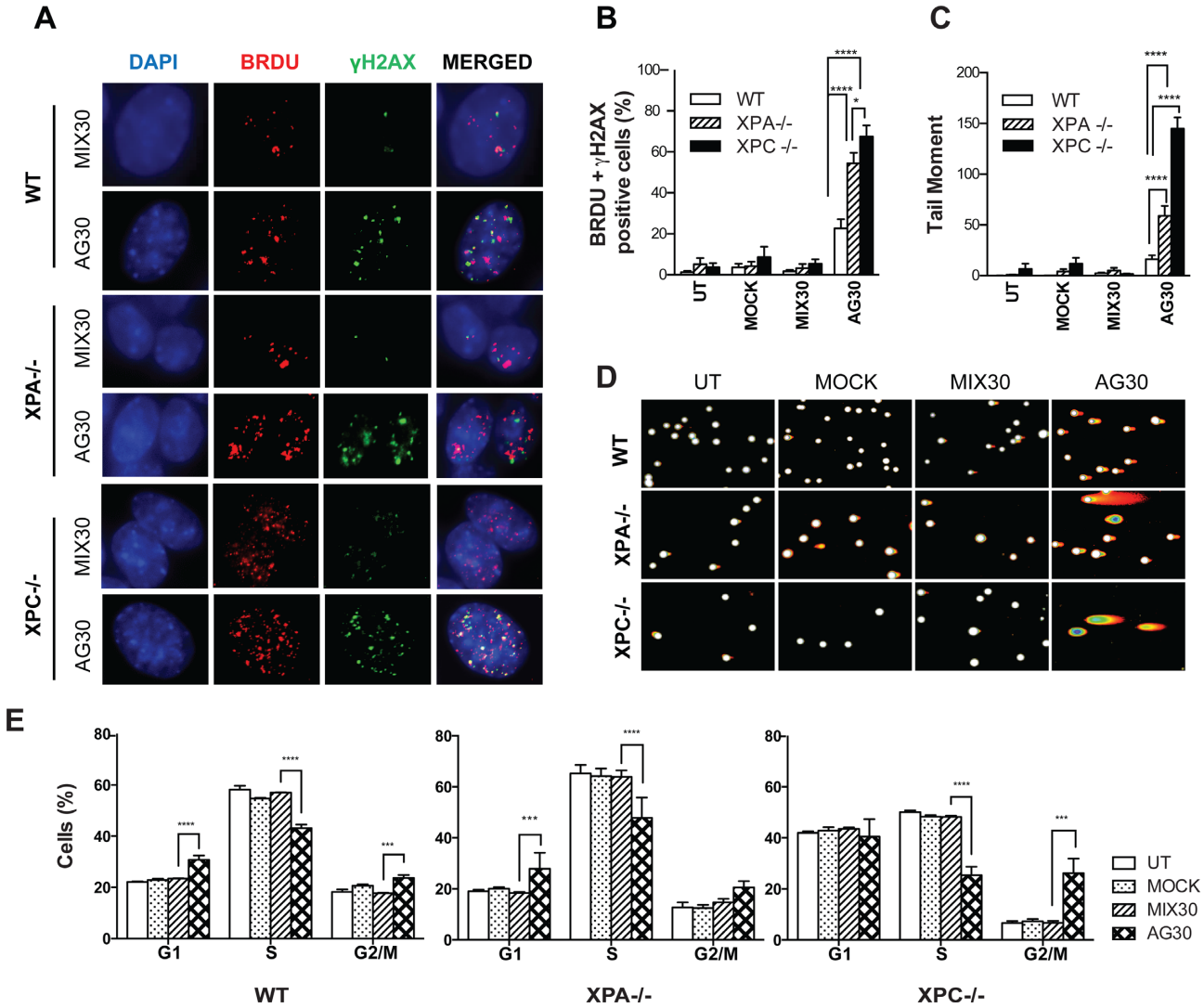

Figure 2. Replication associated triplex-induced DNA strand breaks in NER-deficient cells. (**A**) Immunofluorescence images indicate co-localization of BrdU and γH2AX positive cells. (**B**) Frequency of WT, XPA$^{-/-}$ and XPC$^{-/-}$ (n = 50) cells double-positive for BrdU and γH2AX following 24 h treatment with either the control oligonucleotide, MIX30 or the TFO, AG30. (**C**) Quantification of triplex-induced DNA strand breaks using the alkaline comet assay as measured by tail moment (n = 200). (**D**) Representative images of the alkaline comet assay 24 h post-treatment with MIX30 or AG30. (**E**) Effect of triplex formation on cell cycle progression based on flow cytometry analysis of BrdU incorporation 24 h after TFO-treatment. Statistical significance indicated as *($P < 0.05$), **($P < 0.01$), ***($P < 0.001$) and ****($P < 0.0001$).

cation track length frequency in that range to 66% and 80% in XPA$^{-/-}$ and XPC$^{-/-}$ cells, respectively, compared to 62% in WT cells.

Accumulation of triplex-induced DNA damage at stalled replication forks induces phospho-RPA and Rad51 foci

Stalled replication forks generate long stretches of ssDNA that can trigger RPA phosphorylation, which is required to stabilize the replisome and generate a replication stress response (33–35). To determine if ssDNA levels increased as a result of triplex formation in NER-deficient cells, we conducted immunofluorescence studies of phospho-RPA (pRPA) foci (Figure 4A). In WT and XPA$^{-/-}$ cells, triplex formation induced a small number of large pRPA foci in contrast to XPC$^{-/-}$ cells, which showed numerous but small pRPA foci (Figure 4A). It has been reported that the presence of a few large foci is indicative of late S or G2 cells (36), whereas many small RPA foci is characteristic of cells in mid-S-phase (37). Our data indicate an increase in the mean pRPA foci per cell in AG30-treated cells compared to MIX30-treated cells (Figure 4B). The mean AG30-induced pRPA foci per cell was approximately 2- to 3-fold higher in XPC$^{-/-}$ cells compared to XPA$^{-/-}$ and WT TFO-treated cells. Since RPA is an indicator of regions of ssDNA, these results suggest that the formation of multiple triplex structures induces numerous regions of ssDNA at stalled replication forks, which can result in replication stress. Furthermore, these results imply that generation of single-stranded regions is increased in cells that are unable to recognize the triplex structure as DNA damage.

RAD51 is recruited to sites of damaged replication forks to repair them and restart replication fork progression.

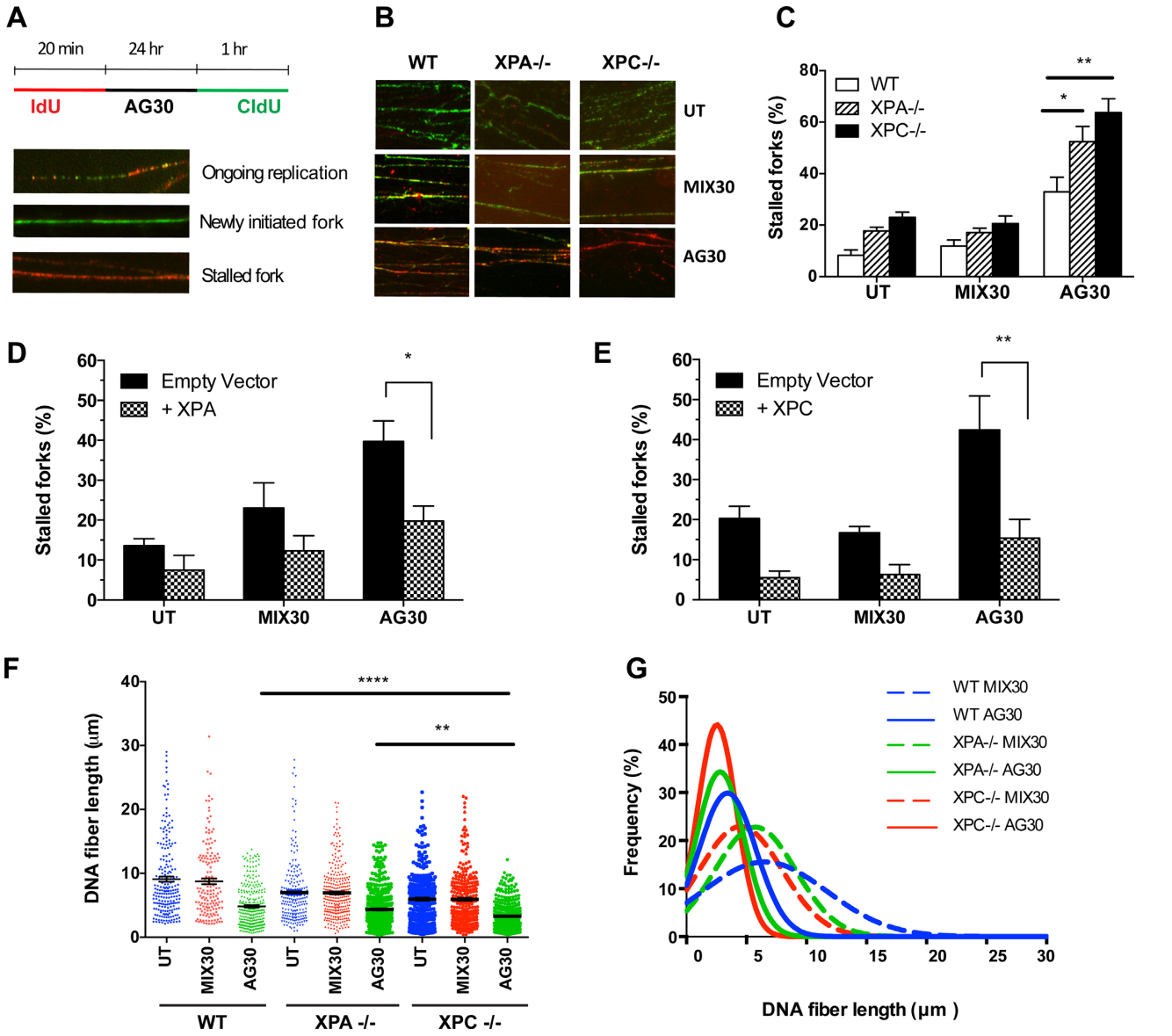

Figure 3. NER proteins XPA and XPC are required for efficient recovery of DNA replication forks after triplex-induced replication stress. (**A**) Schematic describing the DNA fiber assay. Cells were first pulse-labeled with IdU for 20 min and then treated with AG30 or MIX30 for 24 h, followed by CIdU labeling for 60 min. Differential labeling allows for the separation of DNA fibers into three classes. (**B**) Representative images of DNA fibers from WT, XPA$^{-/-}$ and XPC$^{-/-}$ cells after 24 h treatment with either MIX30 or AG30 compared with untreated cells. (**C**) Quantification of stalled replication forks generated 24 h post-treatment with either AG30 or MIX30. (**D**) Quantification of stalled replication forks generated by TFO treatment in XPA$^{-/-}$ cells supplemented with XPA protein compared to cells with vector control. (**E**) Quantification of triplex-induced stalled replication forks in XPC$^{-/-}$ cells complemented with XPC protein. (**F**) DNA fiber length determined for WT, XPA$^{-/-}$ and XPC$^{-/-}$ cells treated with MIX30 or AG30. (**G**) Replication tract length distribution frequency of DNA fibers from AG30- or MIX30-treated WT, XPA$^{-/-}$ and XPC$^{-/-}$ cells. Distribution of replication track length frequency was analyzed based on Gaussian distribution. 250–300 DNA fibers were quantified from three individual experiments. Statistical significance indicated as *($P < 0.05$), **($P < 0.01$), ***($P < 0.001$) and ****($P < 0.0001$).

RAD51 prevents the accumulation of DSBs due to replication stress through homologous recombination when repair of the replication fork fails and results in collapsed forks (30,31). Since we observed replication stress-associated DNA strand breaks, we wanted to explore whether RAD51 interacts at the triplex-induced DNA damage site. To accomplish this, we performed the ChIP assay in WT cells (Supplementary Figure S3A). PCR amplification following chromatin immunoprecipitation with RAD51 antibodies revealed a ∼6-fold enrichment of RAD51 at the TFO binding site 6h post-treatment compared to untreated cells (Supplementary Figure S3B). These results indicate that RAD51 is recruited to the TFO-induced stalled replication fork.

We then proceeded to explore in WT, XPA$^{-/-}$ and XPC$^{-/-}$ cells whether RAD51 colocalizes with γH2AX foci at the sites of DNA damage (Figure 4C). After 24 h of AG30 treatment, all cell lines exhibited an increase in the percentage of RAD51 and γH2AX foci-positive cells. The highest percentage of RAD51- and γH2AX-positive

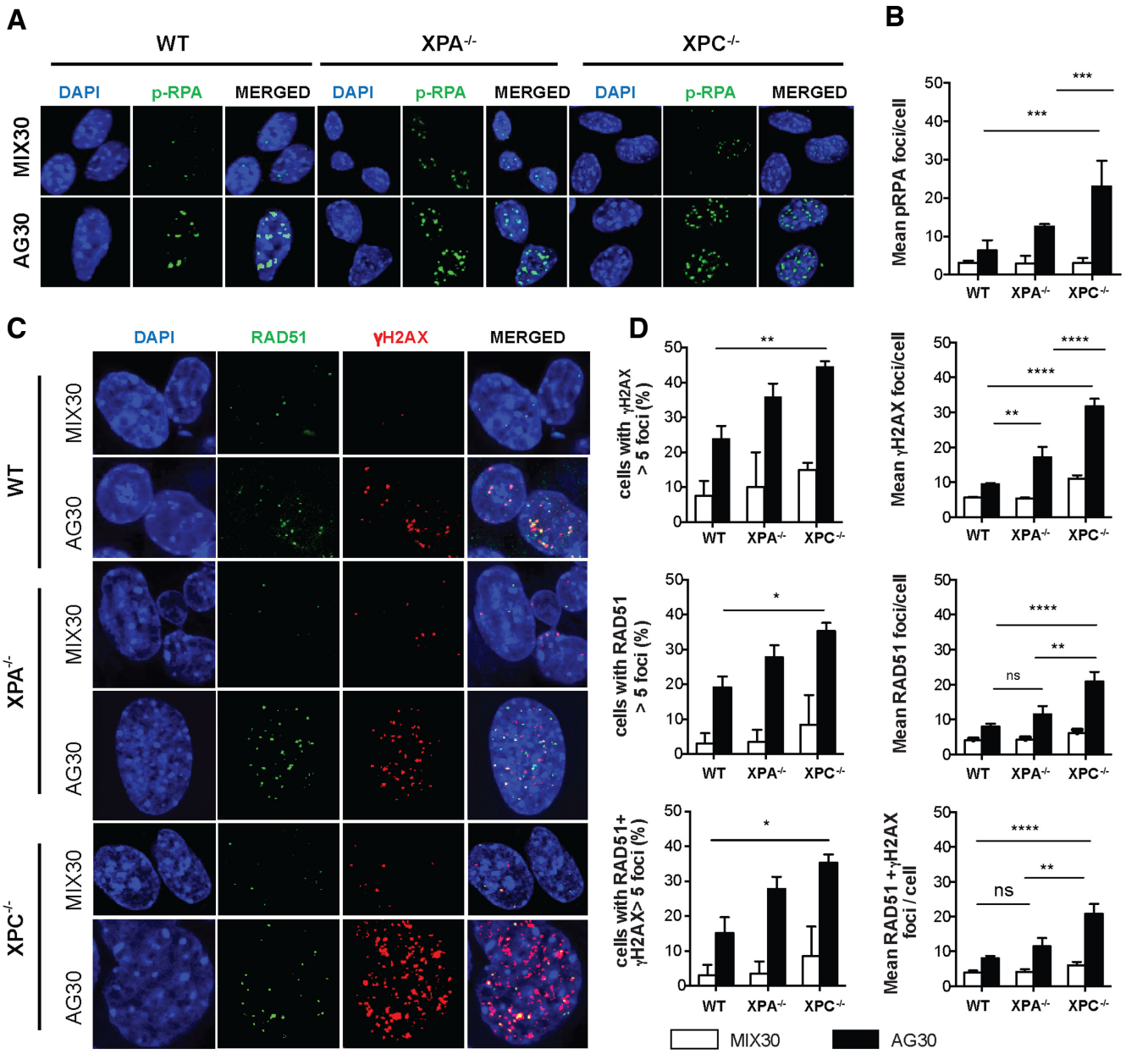

Figure 4. Recruitment of p-RPA and RAD51 following triplex-induced replication stress. (**A**) Immunofluorescence of p-RPA in WT, XPA$^{-/-}$ and XPC$^{-/-}$ cells 24 h post-treatment with MIX30 or AG30. (**B**) Quantification of the mean number of p-RPA foci per cell. (**C**) AG30-induced colocalization of RAD51 foci (green) with γH2AX (red) in nuclei (blue) of WT, XPA$^{-/-}$ and XPC$^{-/-}$ cells as compared to MIX30. (**D**) Quantification of cells with greater than 5 foci, RAD51 and/or γH2AX, per nuclei in WT or NER-deficient cells treated for 24 h with AG30 or MIX30. The results are presented as average ± SEM from two independent experiments. The significant values are represented as *($P < 0.05$), **($P < 0.01$), ***($P < 0.001$) and ****($P < 0.0001$).

cells was observed in XPC$^{-/-}$ (35.3%, 44.6%), followed by XPA$^{-/-}$ (27.7%, 36%) and WT (19.2%, 24%) (Figure 4D). When cells were analyzed for the mean number of RAD51 and γH2AX foci per cell, we observed that formation of multiple triplex structures in the NER-deficient cell lines increased the number of foci. The number of RAD51 foci per cell in AG30-treated XPC$^{-/-}$ and XPA$^{-/-}$ cells was approximately 2 times that of AG30-treated WT cells (Figure 4D). Similarly, there was a greater increase in the number of γH2AX foci per cell in XPC$^{-/-}$ and XPA$^{-/-}$ cells than in WT cells (Figure 4D). Even though the number of RAD51 foci was higher in XPA$^{-/-}$ and XPC$^{-/-}$ than in WT, only partial colocalization of RAD51 foci with γH2AX was observed in these two cell lines compared to NER-proficient cells, where most γH2AX foci were colocalized with RAD51. This observation may be attributed to previous reports indicating that XPC is required for the recruitment of RAD51 to the damage site (38).

Increased DNA damage and the accumulation of DNA DSBs

If they are not repaired in a timely manner, the stalling and collapse of replication forks can lead to DNA DSBs. DSBs are associated with the DNA damage-signaling proteins, γH2AX and 53BP1, which form distinct foci at the DNA damage site. Due to stalled/collapsed replication forks, XPA$^{-/-}$ and XPC$^{-/-}$ cells exhibited larger and more numerous AG30-induced γH2AX- and 53BP1-positive foci than WT cells (Figure 5A). The percentage of 53BP1 foci in AG30-treated XPC$^{-/-}$ cells (46.5%) was higher than in XPA$^{-/-}$ (27.6%) and WT (13.1%) cells, consistent with the percentage of γH2AX-positive cells after AG30 treatment (XPC$^{-/-}$, 59%; XPA$^{-/-}$, 41.3% and WT, 35%, Figure 5B). Colocalization of 53BP1 and γH2AX was observed after AG30 treatment in 43% of XPC$^{-/-}$ cells and 21% of XPA$^{-/-}$ cells compared to 12% of WT cells (Figure 5B). We further assessed the accumulation of DSBs in all cell lines 24 h post-TFO treatment using the neutral comet assay and MIX30, mock and untreated cells as negative controls. The neutral comet assay allows for the quantitative measurement of DNA DSBs by DNA tail moment. AG30 induced DSBs in all cell lines, as shown by an increase in DNA tail moment (Figure 5C and D). Interestingly, untreated XPC$^{-/-}$ cells had ∼4-fold higher tail moment than WT and XPA$^{-/-}$ untreated cells. The highest triplex-induced tail moment was also observed in XPC-deficient cells. These results support our 53BP1 and γH2AX immunofluorescence data, confirming that AG30 induces DNA DSBs as a result of stalled replication. They also reveal that triplex-induced DNA DSBs are not dependent upon the processing of these structures by the NER pathway.

Triplex-induced apoptosis preserves genomic integrity in NER-deficient cells

We have shown that triplex formation generates DSBs in a replication-dependent manner when replication forks encounter the unresolved structures in NER-deficient cells. We then initiated studies to explore whether the replication stress-induced DNA breaks resulted in genomic instability in NER-deficient cells, or whether the accumulation of DNA strand breaks triggered the cells to activate apoptotic pathways as a means to preserve genomic integrity. We measured the level of apoptotic cells 4, 6 and 24 h following AG30-treatment using the AnnexinV assay. We observed AnnexinV-positive cells as early as 6 h, with an increase at 24 h post-treatment (Supplementary Figure S4). TFO treatment induced a significantly higher percentage of apoptosis in XPC$^{-/-}$ cells (66%) compared to XPA$^{-/-}$ (43%) or WT (24%) cells, which correlates with the increased level of DNA damage observed in earlier studies (Figure 6A). Enhanced activation of apoptosis in XPA$^{-/-}$ and XPC$^{-/-}$ cells as a result of triplex formation further suggests that replication forks are unstable and prone to collapse in these repair-deficient cells.

We previously reported that triplex formation induced apoptosis via a signaling mechanism dependent on the phosphorylation of H2AX at S139 and Y142 (25). We wanted to determine if a similar mechanism was utilized in NER-deficient cells. To investigate this, we performed a time course study to observe phosphorylation of H2AX at Y142 and S139. We found that phosphorylation of H2AX at both residues was detectable as early as 4 h post-AG30 treatment in XPA$^{-/-}$ and XPC$^{-/-}$ cells, whereas it was observed 8 h after treatment in WT cells (Figure 6B and C). The dual phosphorylation of H2AX increased 24 h post-treatment in WT cells. As we observed in our previous experiments, triplex-induced DNA strand breaks resulted in the activation of apoptosis in both NER-proficient and NER-deficient cells as determined by the presence of the apoptotic marker, cleaved PARP. Cleaved PARP was detectable at 4 h post-AG30 treatment, with slightly higher levels in the NER-deficient cells. Although cleaved PARP was detectable in both XPA$^{-/-}$ and XPC$^{-/-}$ cells as early as 4 h following TFO treatment, slightly higher levels of S139 phosphorylation were observed in the XPC-deficient cells, suggesting the presence of more DSBs. In the case of XPC$^{-/-}$ cells, an increase in the level of Y142 phosphorylation was detected at the 4 h and 8 h time points compared to XPA$^{-/-}$ and WT cells. As Y142 phosphorylation is a prerequisite for the recruitment of pro-apoptotic proteins, these results correspond with our AnnexinV data.

We wanted to determine whether AG30 treatment induced mutations in cells following the induction of replication-associated DSBs. To accomplish this, we took advantage of an established assay for triplex-induced mutagenesis (14,28,39). The MEF cell lines utilized in this study have multiple copies of the λsupFG1 shuttle vector stably integrated into their chromosomes. *SupFG1* not only contains the AG30 binding site, but also encodes an amber suppressor tRNA whose function can be scored in indicator bacteria. Genomic DNA was isolated from WT, XPA$^{-/-}$ and XPC$^{-/-}$ cells 48 h after mock, MIX30 and AG30 treatment. The vector DNA was then analyzed for induced mutations. In order to evaluate the relevance of apoptosis in preserving genomic integrity, only adherent cells (alive), not floating cells (apoptotic) were collected and analyzed for targeted mutations. We observed an AG30-induced mutation frequency of 27×10^{-5} in WT cells, which was more than 2-fold that of MIX30-treated cells (Figure 6D). Mutation frequency was significantly reduced in AG30-treated XPA$^{-/-}$ cells compared to WT cells (15.9×10^{-5}, Figure 6D), with less than a 2-fold increase compared to MIX30-treated XPA$^{-/-}$ cells. Interestingly, AG30 treatment did not increase mutation frequency in XPC$^{-/-}$ cells (2.9×10^{-5}) compared to MIX30 treatment (12×10^{-5}, Figure 6D). This decrease in mutagenesis corresponds to the increase in apoptosis observed in XPC$^{-/-}$ cells following TFO treatment. Taken together, these results suggest that NER-deficient cells may undergo apoptosis as a means to preserve genomic integrity under conditions where repair is compromised.

The TFO-induced mutations generated in the NER-deficient cell lines were then sequenced to characterize the mutation spectra in the repair-deficient cells (Figure 6E). Sequencing results of the TFO-induced mutations generated in the WT cells revealed 35% insertions, 45% deletions and 20% base substitutions within the triplex target site. Triplex formation in XPA$^{-/-}$ cells resulted in increased insertions (80%), with no alterations in the level of TFO-induced base substitutions. On the other hand, TFO-induced mutations generated in XPC$^{-/-}$ cells resulted in

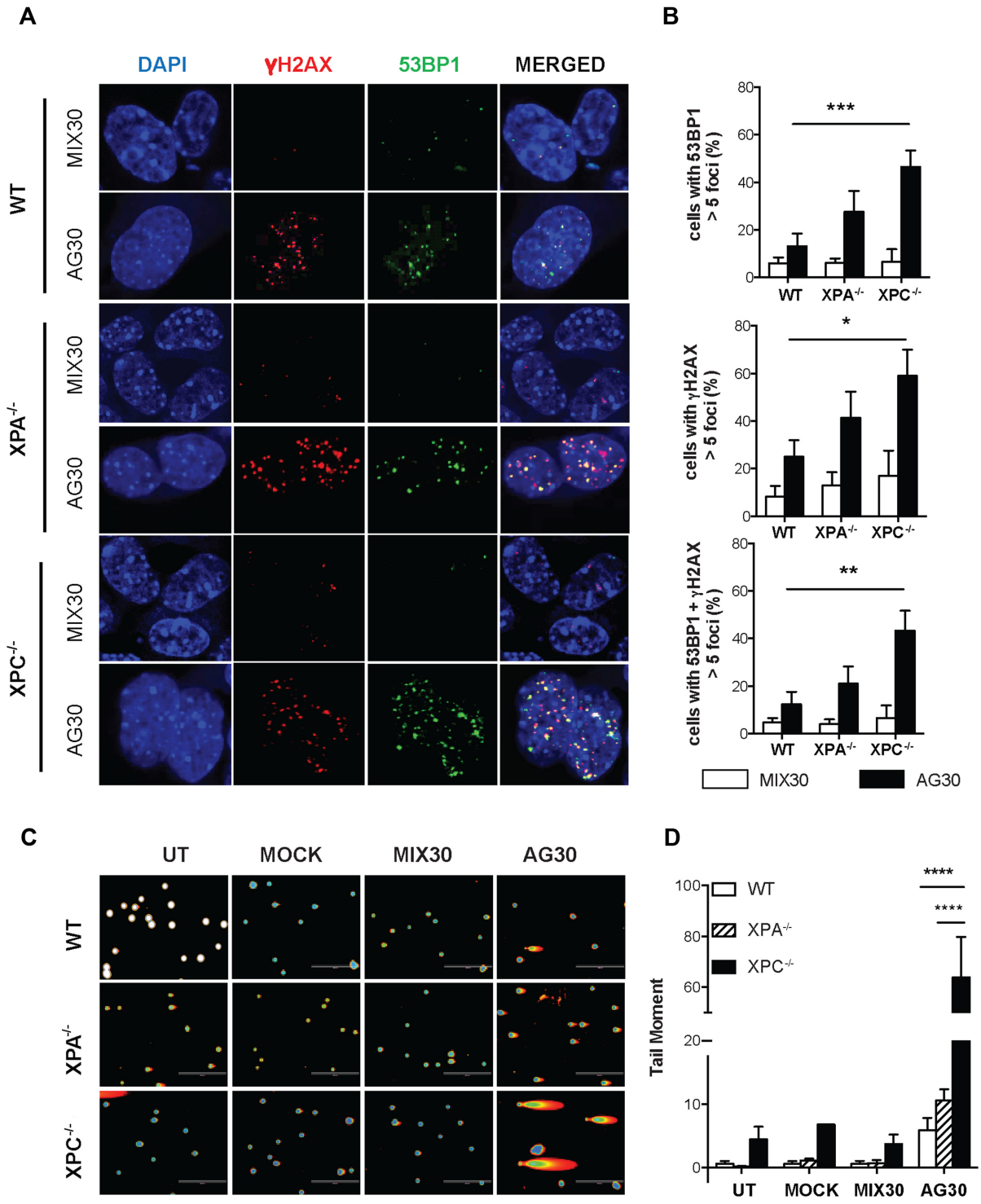

Figure 5. Triplex-induced stalled replication forks result in DNA DSBs. (**A**) Representative images and (**B**) quantification of AG30-induced 53BP1 (green) and γH2AX (red) foci in nuclei (blue) compared to MIX30 24 h post-treatment in WT, XPA$^{-/-}$ and XPC$^{-/-}$ cells. The average percentage ± SEM from two independent experiments is shown. (**C**) Triplex-induced DSBs as measured by neutral comet assay. (**D**) DNA tail moment was used to quantify DNA DSBs induced by 24 h TFO-treatment in WT, XPA$^{-/-}$ and XPC$^{-/-}$ cells. Data represent the mean ± SEM of three independent experiments. A total of 100–200 comets were measured per treatment for each independent experiment. Statistical significance represented as asterisks *($P < 0.05$), **($P < 0.01$), ***($P < 0.001$) and ****($P < 0.0001$).

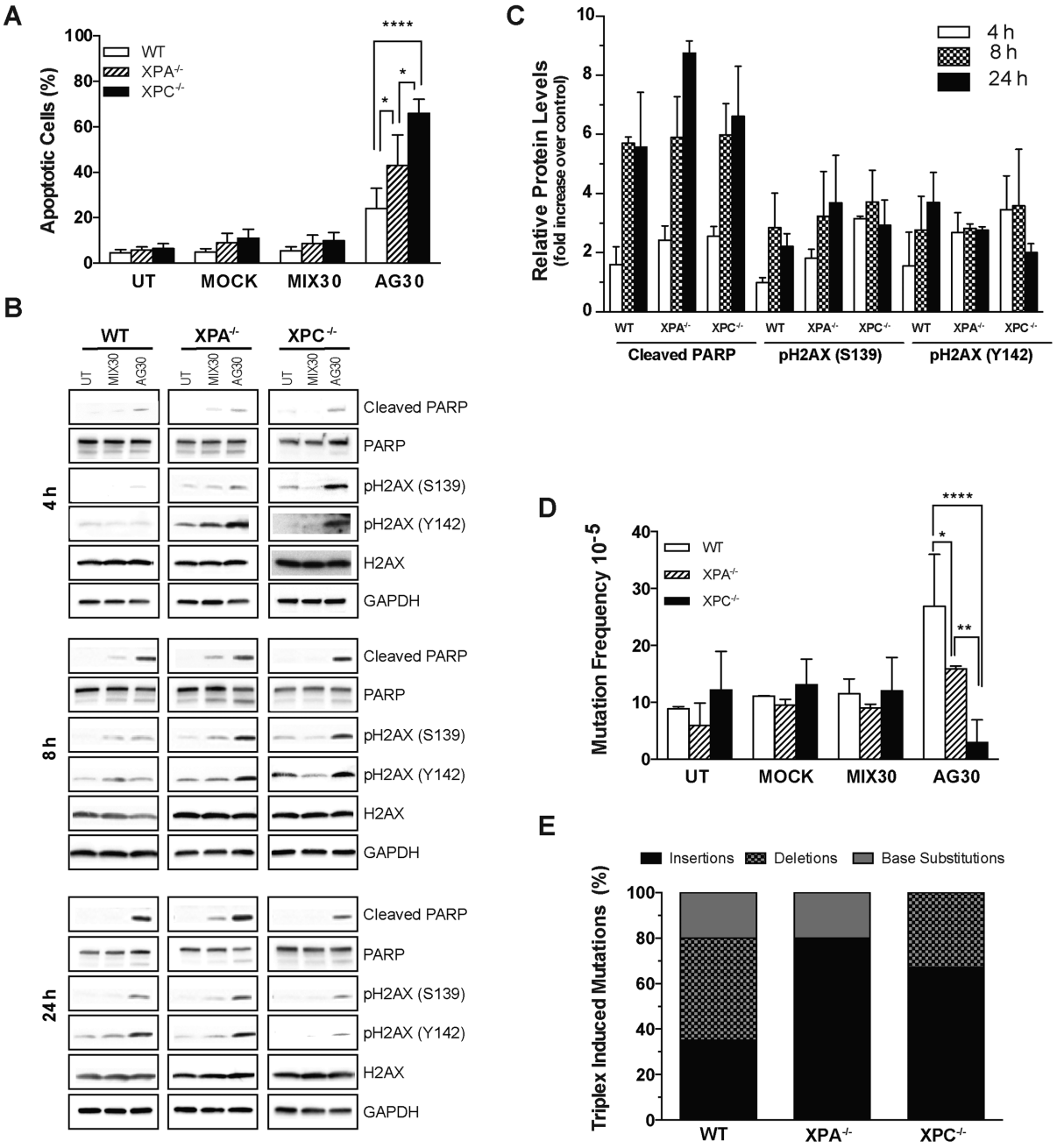

Figure 6. NER-deficient cells preserve genomic integrity through activation of apoptosis. (**A**) Analysis of triplex-induced apoptosis as measured by AnnexinV staining indicates an increase in apoptotic cell death in NER-deficient cells 24 h post-TFO treatment. (**B**) Western blot analysis of the phosphorylation status of H2AX at S139 and Y142 in NER-proficient and -deficient cells following TFO treatment. (**C**) Quantification of Western blot analysis of triplex-induced apoptosis. Results represent three independent experiments. (**D**) Triplex-induced genomic instability as determined by mutation frequencies in the *supFG1* reporter gene in WT, XPA$^{-/-}$ and XPC$^{-/-}$ cells treated with TFOs. Results are from three independent experiments. Two-way ANOVA was used to calculate significant difference *($P < 0.05$), **($P < 0.01$), ***($P < 0.001$) and ****($P < 0.0001$). (**E**) Triplex-induced mutation spectra in NER-proficient and-deficient cells.

an increase in insertions (67%) compared to WT, with 33% deletions and no base substitutions.

DISCUSSION

We previously reported that the formation of multiple triplex structures can activate apoptosis as a result of DNA DSB induction (25). However, the question remained as to the mechanism by which TFOs generate DNA damage. Herein, we have provided evidence that triplex formation causes stalled replication forks and a decrease in the S-phase cell population. In the absence of the NER damage recognition proteins, XPA and XPC, stalled replication forks collapse, resulting in the accumulation of SSBs and DSBs which trigger the cell to activate apoptotic pathways as a

means to preserve genomic integrity. Our findings emphasize the importance of the DNA damage sensor proteins, XPA and XPC in the repair of replication-associated, structurally induced DNA damage. They also suggest a potential role for XPC and XPA in the activation of DNA damage response. These results also provide evidence to support a mechanism where lesion processing is not an essential step for the generation of DSBs following triplex formation. Our results are in contrast to other studies, which report that XPA and XPC are required for γH2AX foci formation and fork breakage following UV irradiation (40).

It has previously been shown by others that DNA replication can be inhibited by sequences that have triplex-forming potential (41,42). However, site-directed inhibition of DNA replication by TFOs has only been demonstrated when the triplex-forming molecules were bound covalently to their target sequences on duplex DNA (11). Our current work demonstrates that the formation of multiple chromosomal triplex structures is capable of stalling replication fork progression. Krasilnikov *et al.* have reported that triplex regions cannot be resolved by DNA polymerase because of increased stability at physiological conditions (43). The replication machinery must be recruited to the triplex site to unravel duplex DNA from triplex DNA.

Triplex formation induces stalled replication forks, DSBs in S phase and G1 cell cycle arrest in XPA$^{-/-}$ cells and G2 arrest in XPC$^{-/-}$ cells. Earlier work determined that the NER proteins, XPA and XPC, recognize triplex DNA (17,21). Although XPC and XPA are both required for DNA damage recognition in the NER pathway, the XPA-RPA complex is not the initial DNA damage recognition factor (44,45). Instead XPA–RPA serves as the 'damage verification' protein in the NER process. Consequently, XPC-hHR23B has been determined to be the initiating factor for damage repair (44). Since XPC is required for DNA damage recognition in the global genome repair (GGR) subpathway of NER, recruitment of the remaining NER proteins to the damage site is inhibited in its absence (40). Lack of damage recognition may explain why we observe more stalled replication forks and DNA breaks in XPC-deficient cells compared to XPA$^{-/-}$ and WT cells. On the contrary, triplex formation in XPA-deficient cells resulted in G1 arrest, which would suggest that the structures are initially recognized as DNA damage. Damage recognition and G1-arrest would allow the cell to repair the structures prior to entry into S-phase. However, in XPA-deficient cells the remaining NER proteins would not be recruited to complete the repair process.

Replication forks can collapse when altered DNA structures are unrepaired, resulting in the formation of DSBs and the potential induction of genomic instability (46–49). To preserve genomic integrity, cells initiate repair of the triplex structure; however, if cells are compromised for repair or overwhelmed by excessive damage, apoptosis is activated (14,24,28). G2/M arrest has been associated with enhanced cell death. In the present study, we demonstrate that triplex formation in XPC-deficient cells triggers G2/M cell cycle arrest and induces apoptosis via a mechanism that includes dual phosphorylation of H2AX at the S139 and Y142 residues. It has been established that the phosphorylation status of the Y142 H2AX residue is critical in determining the relative recruitment of either DNA repair or pro-apoptotic factors to the DSB site (25,50). Although studies suggest that Y142 is gradually dephosphorylated after DNA damage to initiate repair, our current data provides evidence that Y142 is re-phosphorylated to facilitate apoptosis under conditions where repair cannot be completed. In response to the generation of stalled replication forks in XPC-deficient cells, H2AX is phosphorylated at S139 4 h post TFO-treatment, indicating DNA damage. However, 8 h post-treatment, H2AX S139 persists with re-phosphorylation of H2AX Y142. Dual phosphorylation of H2AX on S139 and Y142 activates apoptotic pathways. An apoptotic switch in response to excessive DNA damage in XPC$^{-/-}$ cells prevents the induction of mutations, thus preserving genomic integrity.

SUPPLEMENTARY DATA

Supplementary Data are available at NAR Online.

ACKNOWLEDGEMENTS

We would like to thank R. Jensen for helpful discussions and Y. Lu for helpful guidance with ChIP assays. We also thank P. Glazer for XPA$^{-/-}$ and XPC$^{-/-}$ cells and the XPC expression vector.

FUNDING

National Institutes of Health (NIH) [K22CA120049, K22CA1240049-03S1 to F.A.R.]; Kingsley Fellowship in Medical Research (to F.A.R). Funding for open access charge: Institutional Funds.
Conflict of interest statement. None declared.

REFERENCES

1. Mazouzi,A., Velimezi,G. and Loizou,J.I. (2014) DNA replication stress: causes, resolution and disease. *Exp. Cell Res.*, **329**, 85–93.
2. Boyer,A.S., Grgurevic,S., Cazaux,C. and Hoffmann,J.S. (2013) The human specialized DNA polymerases and non-B DNA: vital relationships to preserve genome integrity. *J. Mol. Biol.*, **425**, 4767–4781.
3. Ciccia,A. and Elledge,S.J. (2010) The DNA damage response: making it safe to play with knives. *Mol. Cell*, **40**, 179–204.
4. Schroth,G.P. and Ho,P.S. (1995) Occurrence of potential cruciform and H-DNA forming sequences in genomic DNA. *Nucleic Acids Res.*, **23**, 1977–1983.
5. Mirkin,E.V. and Mirkin,S.M. (2007) Replication fork stalling at natural impediments. *Microbiol. Mol. Biol. Rev.*, **71**, 13–35.
6. Vasquez,K.M. and Wang,G. (2013) The yin and yang of repair mechanisms in DNA structure-induced genetic instability. *Mutat. Res.*, **743-744**, 118–131.
7. Peleg,M., Kopel,V., Borowiec,J.A. and Manor,H. (1995) Formation of DNA triple helices inhibits DNA unwinding by the SV40 large T-antigen helicase. *Nucleic Acids Res.*, **23**, 1292–1299.
8. Wells,R.D. (2008) DNA triplexes and Friedreich ataxia. *FASEB J.*, **22**, 1625–1634.
9. Shishkin,A.A., Voineagu,I., Matera,R., Cherng,N., Chernet,B.T., Krasilnikova,M.M., Narayanan,V., Lobachev,K.S. and Mirkin,S.M. (2009) Large-scale expansions of Friedreich's ataxia GAA repeats in yeast. *Mol. Cell*, **35**, 82–92.
10. Chandok,G.S., Patel,M.P., Mirkin,S.M. and Krasilnikova,M.M. (2012) Effects of Friedreich's ataxia GAA repeats on DNA replication in mammalian cells. *Nucleic Acids Res.*, **40**, 3964–3974.

11. Diviacco,S., Rapozzi,V., Xodo,L., Helene,C., Quadrifoglio,F. and Giovannangeli,C. (2001) Site-directed inhibition of DNA replication by triple helix formation. *FASEB J.*, **15**, 2660–2668.
12. Krasilnikova,M.M. and Mirkin,S.M. (2004) Replication stalling at Friedreich's ataxia (GAA)n repeats in vivo. *Mol. Cell. Biol.*, **24**, 2286–2295.
13. Ohshima,K., Montermini,L., Wells,R.D. and Pandolfo,M. (1998) Inhibitory effects of expanded GAA.TTC triplet repeats from intron I of the Friedreich ataxia gene on transcription and replication in vivo. *J. Biol. Chem.*, **273**, 14588–14595.
14. Rogers,F.A., Vasquez,K.M., Egholm,M. and Glazer,P.M. (2002) Site-directed recombination via bifunctional PNA-DNA conjugates. *Proc. Natl. Acad. Sci. U.S.A.*, **99**, 16695–16700.
15. de Laat,W.L., Jaspers,N.G. and Hoeijmakers,J.H. (1999) Molecular mechanism of nucleotide excision repair. *Genes Dev.*, **13**, 768–785.
16. Wang,G., Seidman,M.M. and Glazer,P.M. (1996) Mutagenesis in mammalian cells induced by triple helix formation and transcription-coupled repair. *Science*, **271**, 802–805.
17. Vasquez,K.M., Christensen,J., Li,L., Finch,R.A. and Glazer,P.M. (2002) Human XPA and RPA DNA repair proteins participate in specific recognition of triplex-induced helical distortions. *Proc. Natl. Acad. Sci. U.S.A.*, **99**, 5848–5853.
18. Patrick,S.M. and Turchi,J.J. (2002) Xeroderma pigmentosum complementation group A protein (XPA) modulates RPA-DNA interactions via enhanced complex stability and inhibition of strand separation activity. *J. Biol. Chem.*, **277**, 16096–16101.
19. Jeong,Y.T., Rossi,M., Cermak,L., Saraf,A., Florens,L., Washburn,M.P., Sung,P., Schildkraut,C.L. and Pagano,M. (2013) FBH1 promotes DNA double-strand breakage and apoptosis in response to DNA replication stress. *J. Cell Biol.*, **200**, 141–149.
20. Wold,M.S. (1997) Replication protein A: a heterotrimeric, single-stranded DNA-binding protein required for eukaryotic DNA metabolism. *Annu. Rev. Biochem.*, **66**, 61–92.
21. Thoma,B.S., Wakasugi,M., Christensen,J., Reddy,M.C. and Vasquez,K.M. (2005) Human XPC-hHR23B interacts with XPA-RPA in the recognition of triplex-directed psoralen DNA interstrand crosslinks. *Nucleic Acids Res.*, **33**, 2993–3001.
22. Chin,J.Y., Schleifman,E.B. and Glazer,P.M. (2007) Repair and recombination induced by triple helix DNA. *Front. Biosci.*, **12**, 4288–4297.
23. Wang,G. and Vasquez,K.M. (2004) Naturally occurring H-DNA-forming sequences are mutagenic in mammalian cells. *Proc. Natl. Acad. Sci. U.S.A.*, **101**, 13448–13453.
24. Vasquez,K.M., Narayanan,L. and Glazer,P.M. (2000) Specific mutations induced by triplex-forming oligonucleotides in mice. *Science*, **290**, 530–533.
25. Kaushik Tiwari,M. and Rogers,F.A. (2013) XPD-dependent activation of apoptosis in response to triplex-induced DNA damage. *Nucleic Acids Res.*, **41**, 8979–8994.
26. Bindra,R.S. and Glazer,P.M. (2007) Repression of RAD51 gene expression by E2F4/p130 complexes in hypoxia. *Oncogene*, **26**, 2048–2057.
27. Mirzoeva,O.K. and Petrini,J.H. (2001) DNA damage-dependent nuclear dynamics of the Mre11 complex. *Mol. Cell. Biol.*, **21**, 281–288.
28. Rogers,F.A., Manoharan,M., Rabinovitch,P., Ward,D.C. and Glazer,P.M. (2004) Peptide conjugates for chromosomal gene targeting by triplex-forming oligonucleotides. *Nucleic Acids Res.*, **32**, 6595–6604.
29. Jackson,D.A. and Pombo,A. (1998) Replicon clusters are stable units of chromosome structure: evidence that nuclear organization contributes to the efficient activation and propagation of S phase in human cells. *J. Cell Biol.*, **140**, 1285–1295.
30. Petermann,E., Orta,M.L., Issaeva,N., Schultz,N. and Helleday,T. (2010) Hydroxyurea-stalled replication forks become progressively inactivated and require two different RAD51-mediated pathways for restart and repair. *Mol. cell*, **37**, 492–502.
31. Zellweger,R., Dalcher,D., Mutreja,K., Berti,M., Schmid,J.A., Herrador,R., Vindigni,A. and Lopes,M. (2015) Rad51-mediated replication fork reversal is a global response to genotoxic treatments in human cells. *J. Cell Biol.*, **208**, 563–579.
32. Zeman,M.K. and Cimprich,K.A. (2014) Causes and consequences of replication stress. *Nat. Cell Biol.*, **16**, 2–9.
33. Vassin,V.M., Anantha,R.W., Sokolova,E., Kanner,S. and Borowiec,J.A. (2009) Human RPA phosphorylation by ATR stimulates DNA synthesis and prevents ssDNA accumulation during DNA-replication stress. *J. Cell Sci.*, **122**, 4070–4080.
34. Raderschall,E., Golub,E.I. and Haaf,T. (1999) Nuclear foci of mammalian recombination proteins are located at single-stranded DNA regions formed after DNA damage. *Proc. Natl. Acad. Sci. U.S.A.*, **96**, 1921–1926.
35. Liu,S., Opiyo,S.O., Manthey,K., Glanzer,J.G., Ashley,A.K., Amerin,C., Troksa,K., Shrivastav,M., Nickoloff,J.A. and Oakley,G.G. (2012) Distinct roles for DNA-PK, ATM and ATR in RPA phosphorylation and checkpoint activation in response to replication stress. *Nucleic acids Res.*, **40**, 10780–10794.
36. Murphy,A.K., Fitzgerald,M., Ro,T., Kim,J.H., Rabinowitsch,A.I., Chowdhury,D., Schildkraut,C.L. and Borowiec,J.A. (2014) Phosphorylated RPA recruits PALB2 to stalled DNA replication forks to facilitate fork recovery. *J. Cell Biol.*, **206**, 493–507.
37. Dimitrova,D.S. and Gilbert,D.M. (2000) Stability and nuclear distribution of mammalian replication protein A heterotrimeric complex. *Exp. Cell Res.*, **254**, 321–327.
38. Ray,A., Milum,K., Battu,A., Wani,G. and Wani,A.A. (2013) NER initiation factors, DDB2 and XPC, regulate UV radiation response by recruiting ATR and ATM kinases to DNA damage sites. *DNA Rep.*, **12**, 273–283.
39. Gunther,E.J., Yeasky,T.M., Gasparro,F.P. and Glazer,P.M. (1995) Mutagenesis by 8-methoxypsoralen and 5-methylangelicin photoadducts in mouse fibroblasts: mutations at cross-linkable sites induced by offoadducts as well as cross-links. *Cancer Res.*, **55**, 1283–1288.
40. de Feraudy,S., Revet,I., Bezrookove,V., Feeney,L. and Cleaver,J.E. (2010) A minority of foci or pan-nuclear apoptotic staining of gammaH2AX in the S phase after UV damage contain DNA double-strand breaks. *Proc. Natl. Acad. Sci. U.S.A.*, **107**, 6870–6875.
41. Baran,N., Lapidot,A. and Manor,H. (1987) Unusual sequence element found at the end of an amplicon. *Mol. Cell. Biol.*, **7**, 2636–2640.
42. Brinton,B.T., Caddle,M.S. and Heintz,N.H. (1991) Position and orientation-dependent effects of a eukaryotic Z-triplex DNA motif on episomal DNA replication in COS-7 cells. *J. Biol. Chem.*, **266**, 5153–5161.
43. Krasilnikov,A.S., Panyutin,I.G., Samadashwily,G.M., Cox,R., Lazurkin,Y.S. and Mirkin,S.M. (1997) Mechanisms of triplex-caused polymerization arrest. *Nucleic Acids Res.*, **25**, 1339–1346.
44. Li,C.L., Golebiowski,F.M., Onishi,Y., Samara,N.L., Sugasawa,K. and Yang,W. (2015) Tripartite DNA Lesion Recognition and Verification by XPC, TFIIH, and XPA in Nucleotide Excision Repair. *Mol. Cell*, **59**, 1025–1034.
45. Evans,E., Moggs,J.G., Hwang,J.R., Egly,J.M. and Wood,R.D. (1997) Mechanism of open complex and dual incision formation by human nucleotide excision repair factors. *EMBO J.*, **16**, 6559–6573.
46. Ragland,R.L., Patel,S., Rivard,R.S., Smith,K., Peters,A.A., Bielinsky,A.K. and Brown,E.J. (2013) RNF4 and PLK1 are required for replication fork collapse in ATR-deficient cells. *Genes Dev.*, **27**, 2259–2273.
47. Nicolae,C.M., Aho,E.R., Choe,K.N., Constantin,D., Hu,H.J., Lee,D., Myung,K. and Moldovan,G.L. (2015) A novel role for the mono-ADP-ribosyltransferase PARP14/ARTD8 in promoting homologous recombination and protecting against replication stress. *Nucleic Acids Res.*, **43**, 3143–3153.
48. Chanoux,R.A., Yin,B., Urtishak,K.A., Asare,A., Bassing,C.H. and Brown,E.J. (2009) ATR and H2AX cooperate in maintaining genome stability under replication stress. *J. Biol. Chem.*, **284**, 5994–6003.
49. Butin-Israeli,V., Adam,S.A., Jain,N., Otte,G.L., Neems,D., Wiesmuller,L., Berger,S.L. and Goldman,R.D. (2015) Role of lamin b1 in chromatin instability. *Mol. Cell. Biol.*, **35**, 884–898.
50. Cook,P.J., Ju,B.G., Telese,F., Wang,X., Glass,C.K. and Rosenfeld,M.G. (2009) Tyrosine dephosphorylation of H2AX modulates apoptosis and survival decisions. *Nature*, **458**, 591–596.